RSC Advances

PAPER

View Article Online
View Journal | View Issue

Cite this: *RSC Adv.*, 2023, **13**, 5027

Combined molecular dynamics simulations and experimental studies of the removal of cationic dyes on the eco-friendly adsorbent of activated carbon decorated montmorillonite Mt@AC†

Hassan Ouachtak, *[ab] Anouar El Guerdaoui,[c] Rachid El Haouti,[c] Redouane Haounati,[a] Hamza Ighnih,[a] Yahya Toubi,[ab] Fadi Alakhras,[d] Rabia Rehman,[e] Naima Hafid,[f] Abdelaziz Ait Addi*[a] and Mohamed Labd Taha[a]

In recent years, the combination of experimental and theoretical study to explain adsorbate/adsorbent interactions has attracted the attention of researchers. In this context, this work aims to study the adsorption of two cationic dyes, namely methylene blue (MB) and crystal violet (CV), on a green adsorbent Montmorillonite@activated carbon (Mt@AC) composite and to explain the adsorption behavior of each dye by the molecular dynamics (MD) simulation method. The eco-friendly nanocomposite Mt@AC is synthesized and characterized by the analysis methods: XRD, FTIR, BET, TGA/DTA, SEM-EDS, EDS-mapping and zeta potential. The experimental results of adsorption equilibrium show that the adsorption of the two dyes is well suited to the Langmuir adsorption model. The maximum adsorption capacity of the two dyes reaches 801.7 mg g^{-1} for methylene blue and 1110.8 mg g^{-1} for crystal violet. The experimental kinetics data fit well with a pseudo-first order kinetic model for the two dyes with coefficient of determination R^2 close to unity, non-linear chi-square χ^2 close to zero and lower Root Mean Square Error RMSE ($R^2 \rightarrow 1$ and $\chi^2 \rightarrow 0$, RMSE lower). Molecular dynamic simulations are run to gain insights on the adsorption process. According to the RDF analysis and interaction energy calculations, the obtained results reveal a better affinity of the CV molecule with both the AC sheet and montmorillonite framework as compared with MB. This finding suggests that CV is adsorbed to a larger extent onto the nanocomposite material which is in good agreement with the adsorption isothermal experiment observations.

Received 17th December 2022
Accepted 31st January 2023

DOI: 10.1039/d2ra08059a

rsc.li/rsc-advances

1. Introduction

In recent times, environmental management, waste reprocessing, contamination control and wastewater treatment have become the main significant issues all over the world.[1,2] Nations that have experienced water contamination caused by toxic metals, synthetic dyes, organic and metal–organic compounds have faced many troubles, from both financial and ecological perspectives.[3,4]

Synthetic dyes are widely explored in several industries, like: textile, paper, carpet, food, cosmetics, plastic and leather tanning.[5,6] These complex materials are discharged into the aqueous effluents causing pollution and environmental crisis.[7] Synthetic dyes generally have complex aromatic structures based on hydrocarbon moieties such as benzene, toluene, xylene, naphthalene, *etc.* The complex nature of these dyes makes them more stable and non-biodegradable.[8] Additionally, dyes are toxic, carcinogenic and mutagenic molecules causing serious destruction of the kidneys, liver, brain, fertility and central nerve system.[9] Accordingly, it is very important to manage the amount of toxic dyes in wastes before flowing into the environmental system.

Various treatment methods are improved to dyes removal from industrial effluents. For instance: biological treatment, membrane separation, aerobic coagulation, oxidation and electrochemical techniques are extensively used.[10–13] However, the adsorption method is considered as one of the universal approaches utilized for the removal of toxic organic and inorganic poisons due to its simplicity, feasibility, and effective

[a]*Laboratory of Organic and Physical Chemistry, Faculty of Science, Ibn Zohr University, Agadir, Morocco. E-mail: ouachtakhassan@gmail.com; aitaddi.abdelaziz@gmail.com*

[b]*Faculty of Applied Science, Ait Melloul, Ibn Zohr University, Agadir, Morocco*

[c]*Department of Chemistry, Faculty of Science, Ibn Zohr University, Agadir, Morocco*

[d]*College of Pharmacy, Middle East University, Amman, 11831, Jordan*

[e]*Institute of Chemistry, University of the Punjab, Lahore, 54590, Pakistan*

[f]*Regional Center of Education and Training Souss Massa, Morocco*

† Electronic supplementary information (ESI) available. See DOI: https://doi.org/10.1039/d2ra08059a

sorption ability.[14,15] Different types of adsorbent materials are used effectively in removing of colored dyes from aqueous solutions. Nevertheless, sometimes the costly associated processes for the renewal and reprocess of the adsorbents warrant the researchers toward investigating alternative low-cost sorbent materials. There are different types of low cost sorbent materials such as: dead bio-mass, seaweed, mesoporous silica SBA-15, natural zeolite, mineral clay, and agricultural waste.[16] Activated carbons (ACs) have gained increasing interest because these materials have broad range of industrial applications including gas and air cleaning.[17] Furthermore, ACs are widely used in the treatment, purification and decolorization of wastewater.[18] This process has particular significance in the pharmaceuticals, beverage, food and other industrial waste treatment plants. Activated carbon-based materials have high specific surface area and well-allocated pore volumes with the existence of some electron donor functional groups (hydroxyl, carboxyl, phenol, quinine and lactone) on the surface which are obtained from the feedstock materials. These functional groups are responsible for removing contaminants which makes ACs more effective toward different types of inorganic or organic pollutants discharging in aqueous solutions.[19] Activated carbons can be obtained by chemical or physical activation process. The physical one includes the pyrolysis of the stock material and the pyrolytic char is activated in steam or carbon dioxide.[20] Chemical process can be performed in a single step by executing the pyrolysis of precursor in the presence of chemical activating reagents with an inert atmosphere.[19] However, chemical activation process is more preferable due to its low energy demand and operating cost, more carbon percentage yields and larger surface area.[21]

Recently, locally available and less expensive carbonaceous precursors are widely utilized in producing of ACs due to environmental, economic and societal perspectives. Different agricultural wastes such as peanut hulls, corncobs, coffee beans, cotton stalk, grape seeds and pistachio wood[16] have been exploited as precursors for activated carbons.

On the other hand, clay minerals and their tailored derivatives have composed an outsized family of sorbents which could be utilized for the removal of diverse contaminants from solution.[14,22] Among this family, montmorillonite is considered as one of the most adsorbent materials because it is naturally available, has good adsorption capacity, physical and chemical properties, inexpensive, good cation exchange capacity and high superficial area.[7,14,22]

The main objective of this work is to develop a carbon-based nano-clay composite material for the treatment of contaminated water. For this, we exploit the Moroccan clay and wheat straw (WS) as the main bio-waste to develop a Montmorillonite-activated carbon (Mt@AC) composite material to exploit the interlayer structure of montmorillonite and the porosity of AC. This nanocomposite is a low-cost eco-friendly adsorbent material used for the removal of toxic cationic dyes from wastewater. The morphological and structural properties of prepared composite were characterized by different analysis techniques, such as: Fourier transform infrared (FT-IR) spectroscopy, thermogravimetric analysis/differential thermal analysis TGA/DTA, X-ray diffraction (XRD), zeta potential, Scanning electron microscopy (SEM), energy dispersive X-ray spectroscopy and nitrogen (N_2) sorption (BET method). Batch adsorption tests were performed to find out the performance of the composite to adsorbed cationic dyes such as methylene blue and crystal violet. In addition, the Molecular dynamics (MD) is a very useful tool for better understanding of the adsorption mechanisms regarding the structural and energetic information. This information can be obtained from analyzing conformational rearrangements of compounds as well as interactions that occurred amongst the different components of a molecular system. In the present work, the adsorption process of the CV and MB organic dyes onto the Mt@AC composite material is theoretically analyzed using molecular dynamics method to assess the affinity and intermolecular interactions of the investigated dyes toward the synthesized nanomaterial.

2. Materials and methods

2.1. Chemicals and materials

The details of the origin and the type of montmorillonite (Mt) used in this work were published in our previous work[1,7,14] All chemicals and reagents were of analytical grade and obtained from Sigma Aldrich. Crystal violet (CV) ($C_{25}H_{30}N_3Cl$; molecular weight: 408 g mol^{-1}, molecular color in λ_{max} = 590 nm, solubility aqueous: 10 g); methylene blue ($C_{16}H1_8ClN_3S$; molecular weight: 319.9 g mol^{-1}, molecular color in λ_{max} = 661 nm, solubility aqueous: 10 g L^{-1}); sodium hydroxide NaOH (molecular weight 39.99 g mol^{-1}, 98%) and hydrochloric acid HCl (molecular weight 36.46 g mol^{-1}, 37%).

2.2. Preparation of Mt@AC composite

The montmorillonitet@activated carbon composite has been prepared by a simple and eco-friendly method.

2.2.1. Preparation of activated carbon. Typical synthetic process was applied as follows: 20 g of the wheat straw was mixed with a solution of phosphoric acid 60% H_3PO_4 of volume of 200 mL, the mixture was stirred at a temperature of 80 °C for 4 h to ensure the reaction between phosphoric acid and wheat straw. Then, the obtained solid was separated and dried at 90 °C overnight and was charred at 600 °C in a muffle furnace for 1 h with a heating rate of 10 °C min^{-1}.

2.2.2. Preparation of montmorillonite@activated carbon. The Montmorillonite@activated carbon (Mt@AC) composite was prepared by the heterogeneous suspension reaction process where the Mt particles were mixed with the prepared AC. In a typical preparation, 5 g of Mt mineral clay sieved through <50 μm and then was dispersed in a volume of 200 mL of demineralized water in an ultrasonic bath for 2 h. After that, 5 g of prepared AC with powder size of <50 μm was added to the clay slurry and stirred for 3 h at a temperature of 80 °C. Finally, the solid composite was obtained from the solution by filtration and dried at 90 °C for 12 hours.

2.3. Characterization

More detailed characterizations are presented in the ESI S1.†

2.4. Adsorption tests

The Mt@AC composite was tested for the removal of crystal violet (CV) and methylene blue (MB) dyes from aqueous solutions at room temperature (20 °C ± 0.5 °C) using batch technique. The adsorption trials were performed using a number of glass bottles (200 mL) containing the desired dose of Mt@AC adsorbent and 100 mL of CV or MB solution with a known concentration. The glass bottles were agitated at constant speed of 150 rpm. Finally, after each adsorption test, the liquid phase was obtained using a Millipore membrane filter (0.45 μm) and the amount of dye in each samples was measured using UV-visible spectrophotometer (UV-1800, SHIMADZU).

The effect of the adsorbent dosage on the adsorption of CV and MB dyes was tested over the Mt@AC adsorbent dosage range of 0.2 to 1.2 g L^{-1}; the glass vials were shaken for 2 h to ensure equilibrium. The effect of pH on the adsorption process was investigated at different pH values between 2.0 and 10.0 where the pH value of the solutions was adjusted using 0.1 mol L^{-1} HCl or 0.1 mol L^{-1} NaOH. For kinetic studies, the effect of contact time (5 to 180 min) was calculated for each dye at three initial concentrations (150, 250 and 400 mg L^{-1}). The adsorption isotherm studies for each dye were also performed by shaking 1.0 g L^{-1} of Mt@AC with 100 mL of dye solution at initial concentrations ranging from 500 to 1500 mg L^{-1} for CV dye and 200 to 1250 mg L^{-1} for MB dye for 120 min.

Adsorbed quantities of dye Q_t (mg g^{-1}) at different time t or Q_e (mg g^{-1}) at diverse initial concentrations were evaluated using eqn (1). The % Removal for the adsorption process was estimated using eqn (2).

$$Q_{e,t} = \frac{(C_0 - C_{e,t}) \times V}{m} \quad (1)$$

$$\%\ \text{Removal} = \frac{(C_0 - C_{e,t})}{C_0} \times 100 \quad (2)$$

where C_0 (mg L^{-1}) is the initial adsorbate concentration, C_t (mg L^{-1}) and C_e (mg L^{-1}) are the equilibrium concentration at diverse times and equilibrium concentration at different initial dye concentrations, respectively. V (L) is the solution volume, m (g) is the mass of the Mt@AC adsorbent.

2.5. Analysis data

The mathematical equations corresponding to the different adsorption isotherm models and the kinetic models as well as the errors functions are summarized in Table 1.

3. Results and discussion

3.1. Characterization

3.1.1. FTIR analysis. The FTIR spectra of Mt compared with activated carbon and modified Mt@AC are recorded in the region of 4000–400 cm^{-1}. As can be depicted in Fig. 1, typical bands of montmorillonite clay minerals are clearly observed. Presence of adsorption band around 1649 cm^{-1} and 3435 cm^{-1} corresponds to the stretching vibration of hydroxyl groups O–H of water molecules that are present in the hydrogen bonded interlayer. Meanwhile, the absorption band located at 3629 cm^{-1} is due to the interaction of hydroxyl group OH^- with aluminum and silicon ions (Al–OH and Si–OH).[30] The strong characteristic absorption peak at 1030 cm^{-1} is assigned to the Si–*O*–Si stretching vibration. Then, the bands around 472 cm^{-1} and 793 cm^{-1} can also be attributed to Si–*O*–Si and Si–O deformation respectively, whereas the two small absorption bands at 534 cm^{-1} and 660 cm^{-1} are ascribed to Si–O–Al

Table 1 The equations of kinetics models, isotherms models and error functions[a]

Isotherm model or kinetic model	Equations	Reference
Pseudo first order	$Q_t = Q_{e,1}(1 - e^{k_1 t})$, eqn (3)	23
Pseudo second order	$Q_t = \frac{Q_e^2 k_2 t}{1 + k_2 Q_{e,2} t}$, eqn (4)	24
Freundlich isotherm	$Q_e = K_F C_e^{1/n}$, eqn (5)	25
Langmuir isotherm	$Q_e = \frac{Q_m K_L C_e}{1 + K_L C_e}$, eqn (6)	26

Error functions

Error function	Equation	Reference
Chi-squared	$\chi^2 = \sum \frac{(Q_{e,exp} - Q_{e,cal})^2}{Q_{e,cal}}$, eqn (7)	27
Coefficient of determination R^2	$R^2 = 1 - \frac{\sum (Q_{e,exp} - Q_{e,cal})^2}{\sum (Q_{e,exp} - Q_{e,mean})^2}$, eqn (8)	28
Residual root mean square error RMSE	$\text{RMSE} = \sqrt{\frac{1}{n-2} \sum (Q_{e,exp} - Q_{e,cal})^2}$, eqn (9)	29

[a] Notation: Q_t (mg g^{-1}) and Q_e (mg g^{-1}) are the adsorbed quantities at time t (min) and equilibrium, respectively. k_1 (min^{-1}) and k_2 (mg g^{-1} min^{-1}), are the rate constants of pseudo-first order and pseudo-second order, respectively. C_e (mg L^{-1}) is the equilibrium concentration, Q_m is the maximum adsorbed quantity (mg g^{-1}), K_L is the Langmuir constant (L mg^{-1}). K_F (mg g^{-1}) (mg L^{-1}) ^{n} is the Freundlich isotherm constant; n is the heterogeneity factor; $Q_{e,exp}$ (mg g^{-1}) is the adsorbed quantity obtained experimentally, $Q_{e,cal}$ (mg g^{-1}) is the adsorbed quantity obtained from the kinetic model or isotherm adsorption model by using the Solver add-in "in Microsoft Excel", $Q_{e,mean}$ (mg g^{-1}) is the mean of the values of $Q_{e,exp}$. N is the number of observations in the experimental data.

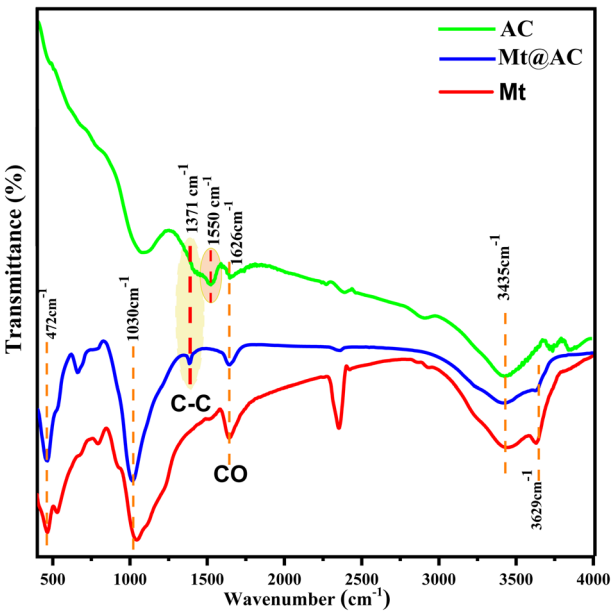

Fig. 1 FT-IR spectra of Mt, AC and Mt@AC.

bending vibrations and Al–O vibrations, respectively.[31] On the other hand, the FTIR spectra of activated carbon show the wavenumber near 1371 cm^{-1} could be attributed to –C–C– stretching vibrations of bonds of carbon. Thus, the FTIR spectrum of montmorillonite clay shows the same stretching and bending obtained by previous studies.[32–34] In the spectrum of Mt@AC, it can be observed the appearance of only one absorption band at the 1373 cm^{-1} which is assigned to anti-symmetric stretching vibration characteristic for the C–C bonds of carbon.[35] Moreover, the band observed at 1626 cm^{-1} is typically associated with the presence to the C=O stretching vibrations of carbonyl and carboxyl groups.[36] In addition, the band located at 1550 cm^{-1} is related to the C=C stretching vibration.[37]

3.1.2. XRD analysis. The XRD patterns of Mt, Mt@AC, Mt@AC/CV and Mt@AC/MB powders are displayed in Fig. 2. As can be observed, the characteristic peaks of the crystalline phase of Mt are located at $2\theta = 7.303°$ ($d_{001} = 1.209$ nm, the parallel interlayers in the Mt clay mineral), 19.77°, 20.83°, 26.61° and 35.02°. Both quartz and calcite are identified as minor impurities. The XRD patterns of Mt@AC composite show that the d_{001} reflection of montmorillonite remains unchanged after modification with activated carbon. This can affirm that activated carbons do not make any change in the basal spacing of montmorillonite during the course of synthesizing process. However, few peaks are disappeared. This can be explained by covered partial surface of clay mineral by AC. Finally, the adsorption of both MB and CV dyes reveals that parallel-interlayers structure of clay mineral increased significantly which are reached $d_{001} = 13.36$ Å at $2\theta = 6.61°$ and $d_{001} = 14.04$ Å at $2\theta = 6.28°$ respectively.

3.1.3. BET analysis. The nitrogen adsorption–desorption measurements at 77 K are used to study the surface area and pore structure of Mt and Mt@AC. In Fig. 3a, the materials show type IV isotherm with H3 hysteresis loop consistent with International Union of Pure and Applied Chemistry classification, which ascribes the presence of pore and mesoporous category of material.[38] The textural properties of both samples are determined and presented in Table 2. The Brunauer–Emmett–Teller (BET) surface areas of Mt and Mt@AC are 76.65 and 199.64 $m^2\ g^{-1}$, respectively. Meanwhile, the BJH graph (Fig. 3b) shows the pore volume and average pore diameter of Mt and Mt@AC which are found to be (0.0012 $cm^{-3}\ g^{-1}\ Å^{-1}$ and 18.69 $Å^{-1}$) and (0.0024 $cm^{-3}\ g^{-1}\ Å^{-1}$ and 18.80 $Å^{-1}$) respectively. The large specific surface area and increased pore volume of Mt@AC compared with Mt can be attributed to the disordered of layers in Mt@AC, which is due to the intercalation of the carbonaceous materials into the interlayer region of Mt. Furthermore, the synergic effect between Mt and carbon has a very important role on the specific surface area and porosity of the Mt@AC composite leading to be a better alternative adsorptive material for removal of toxic dyes in wastewater.

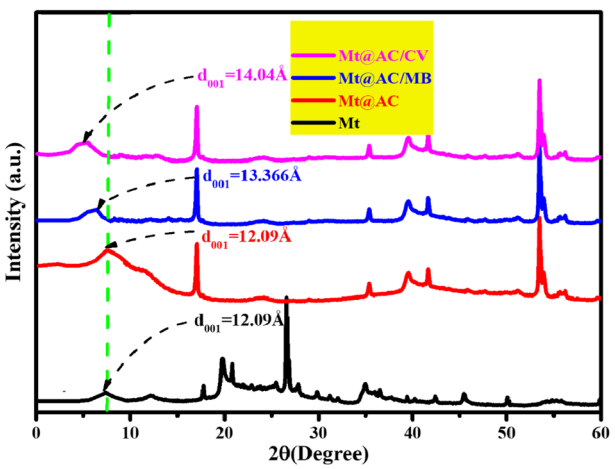

Fig. 2 XRD patterns of Mt and Mt@AC, Mt@AC/CV and Mt@AC/MB.

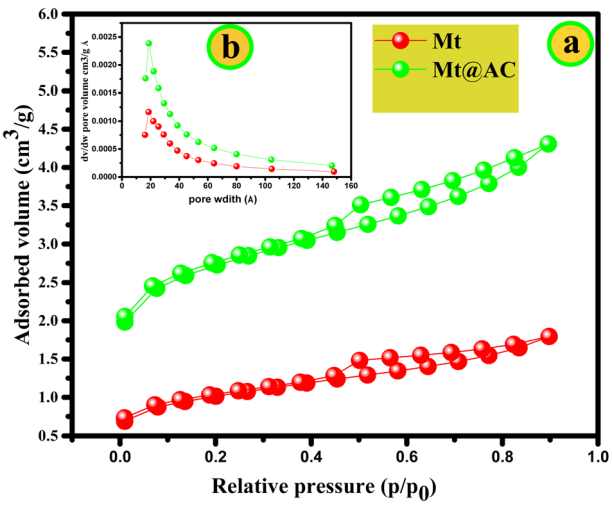

Fig. 3 The nitrogen adsorption–desorption isotherm at 77 K (a) and pore size distribution curve (b) of Mt and Mt@AC composite.

Table 2 BET surface area, pore volume and pore size values of Mt and Mt@AC composite

Sample name	BET surface area A_{BET} ($m^2\ g^{-1}$)	Differential pore volume ($cm^{-3}\ g^{-1}\ Å^{-1}$)	Pore size ($Å^{-1}$)
Mt	76.6531	0.0012	18.69
Mt@AC	199.6442	0.0024	18.80

3.1.4. TGA/DTA analysis. The thermal stability of Mt activated carbon and Mt@AC is determined by thermal gravimetric analysis (TGA) and derived thermogravimetric (DTA) in the temperature range from 25 °C to 1000 °C. Fig. 4a–c represent the DTA and TGA diagrams of the Mt, activated carbon and Mt@AC, respectively.

For three samples, a mass loss of 4.30% is observed for Mt, 4.14% for activated carbon and 4.15% for Mt@AC in the temperature range 25–130 °C corresponds to surface water. In parallel At the same time, the DTA analyzes of three samples shows an endothermic thermal process around 95 °C. A second loss of mass is observed with 3.11% for Mt, 35.98% for activated carbon and 5.31% for Mt@AC in the temperature range (≈130 °C – 800 °C) which is corresponding to the dehydration of intercalated water and exchangeable cations at interlayer space of the montmorillonite. The significant mass loss of the activated carbon could which is due to the easy to degradation of bonds carbon at high temperature compared to the Mt@AC sample (−5.31%) and the Mt (−3.11). The last loss of mass is recorded after 800 °C of the Mt and Mt@AC samples; 1.75% for Mt and 1.38% for Mt@AC can be attributed to the dehydroxylation of the silanol groups Si–OH and of the aluminol groups Al–OH of the montmorillonite. The results of thermogravimetric analysis show that Mt@AC composite is stable in the temperature range 20 °C–1000 °C with a total mass loss of ≈10%.

3.1.5. Surface morphology. The morphology and surface elements of Mt and Mt@AC are tested by scanning electron microscopy and energy dispersive X-ray spectroscopy. The SEM images of Mt have already been published in our previous work[1,7,39] The morphology of Mt is in the shape of nanosheets confirms the structure of the montmorillonite clay mineral, and EDS analysis shows that the elements silicon, magnesium and oxygen are presented at significant percentages on the surface of Mt. Concerning the Mt@AC composite prepared in this work, the results of SEM and EDS analyzes are presented in Fig. 5. From this figure, the composite comprises the two structures of montmorillonite and AC. The image in Fig. 5b shows that montmorillonite retains its initial shape with AC particles deposited on its surface. In Fig. 5c, the structure of the AC is clearly shown, which proves the success of the preparation of the composite Mt@AC. Also, pores are observed (Fig. 5c) which is corresponding to the micropore structure of AC that could improve the adsorption of dyes by the composite. The preparation of the Mt@AC composite composed of clay and AC gives the surface a chemical and very reactive heterogeneity and has the both of AC functions (carboxyl groups –COOH and hydroxyl groups –OH) and functional groups of clays (aluminol groups

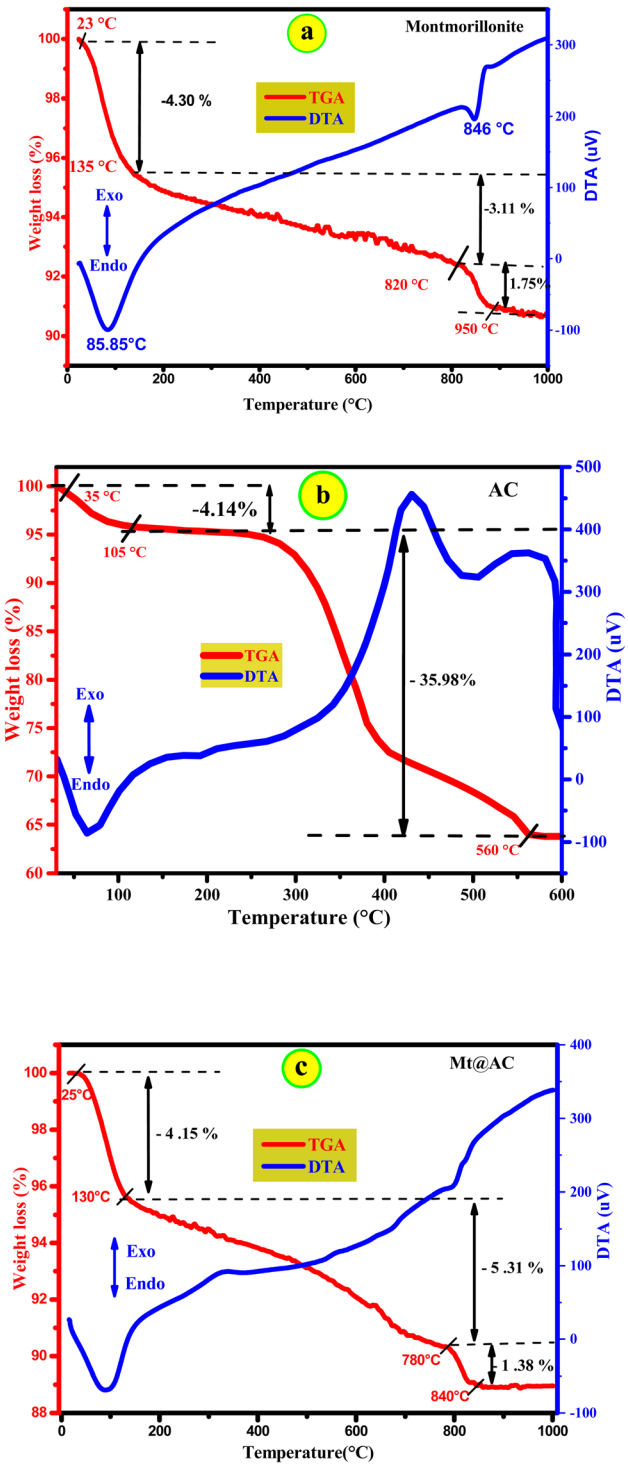

Fig. 4 TGA/DTA diagrams of (a) Mt, (b) activated carbon and (c) Mt@AC.

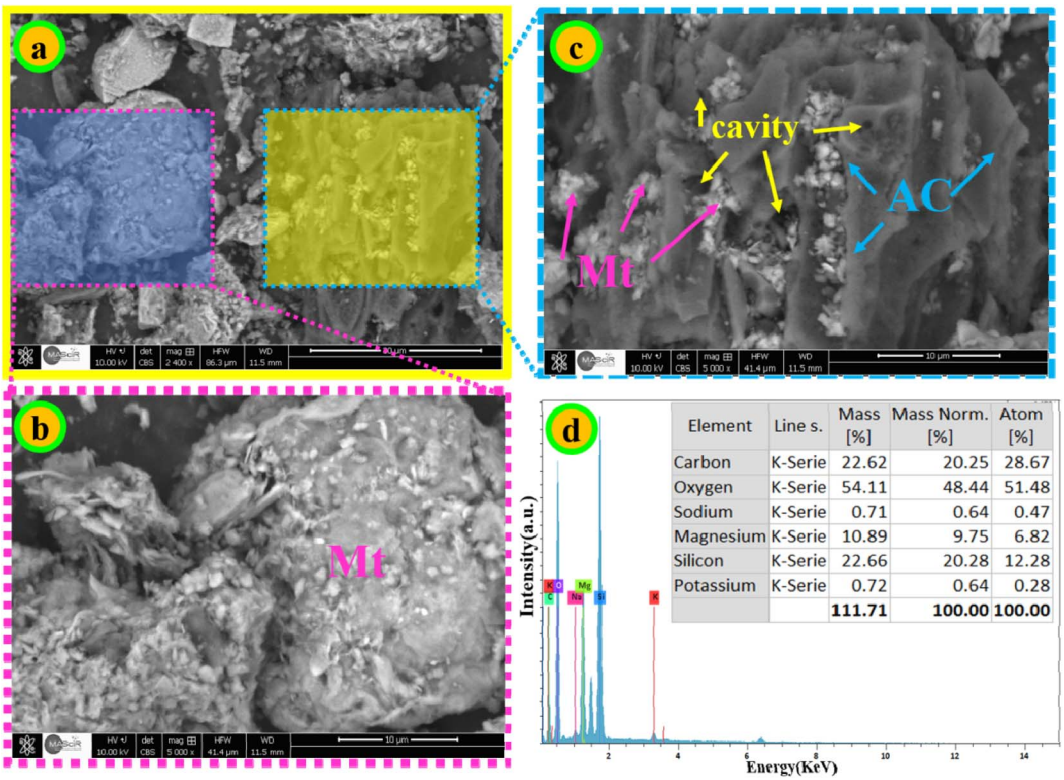

Fig. 5 SEM-EDS of Mt@AC with various resolutions.

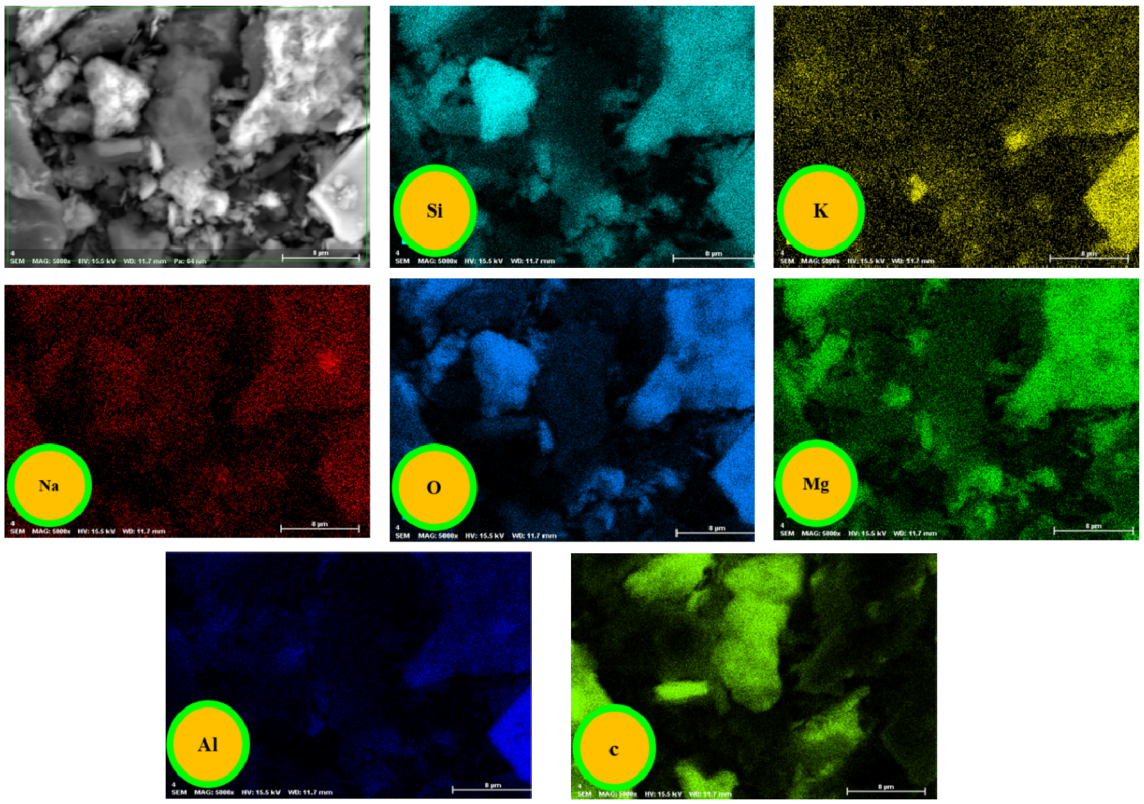

Fig. 6 EDS elemental mapping of Mt@AC.

Al–OH and silanol groups Si–OH). The chemical heterogeneity of the Mt@AC component surface is confirmed by EDS analysis. The EDS spectrum in Fig. 5d shows extremely high peaks for silicon, carbon and magnesium, which confirms the elemental composition of composite consisting of clay and AC. The SEM-EDS elemental mapping analysis of the Mt@AC composite presented in Fig. 6 shows the distribution of the chemical elements silicon, aluminum, carbon, oxygen, magnesium, sodium and potassium on the surface of the composite which also confirms the results of SEM analysis.

3.2. Adsorption process

3.2.1. Effect of adsorbent dose. The influence of adsorbent dose (Mt@AC) on the removal of each dyes MB and CV separately at natural pH from its aqueous solution is demonstrated in Fig. 7. The initial dyes concentration is 100 mg L^{-1} and the adsorbent dosage of the Mt@AC is varied from 0.2 to 1.2 g L^{-1}. From Fig. 7, it can be seen that the removal efficiency of dyes (MB and CV) increases relatively rapidly with the rise of adsorbent dose (Mt@AC) from 0.2 to 1 g L^{-1} where the removal percentage of dyes increases from 79 to 98.58% and from 80 to 99.5% for MB and CV, respectively. After 1 g L^{-1} the removal percentage of dye is approximately invariable. This increase of the removal efficiency with increasing sorbent dosage can be indicated to the increasing number of adsorption sites on the sorbent surface and the increase of the surface area of Mt@AC adsorbent.[40,41] At the same time, the adsorbed MB and CV amount will increase steadily with declining the Mt@AC. According to that, the highest removal percentage of the Mt@AC is achieved at 1 g L^{-1}, which is effectively removed (98.58% for MB and 99.5% for CV) is selected as the optimal dosage and used in the subsequent experiments.

3.2.2. Effect of pH. The effect of pH in aqueous solution is an investigating effective parameter that affects the interfacial transport phenomena, functional groups of the adsorbent surface[15] and thereby affects the adsorption behaviors.[42] To study the effect of pH of the initial solution on the adsorption capacity of both dyes (MB and CV), experiments were performed with 1 g of Mt@AC, while keeping the concentration of 100 mg L^{-1} of each dye (MB and CV separately) at 20 °C and a contact time of 2 h and over a wide pH range from 2 to 12 (Fig. 8).

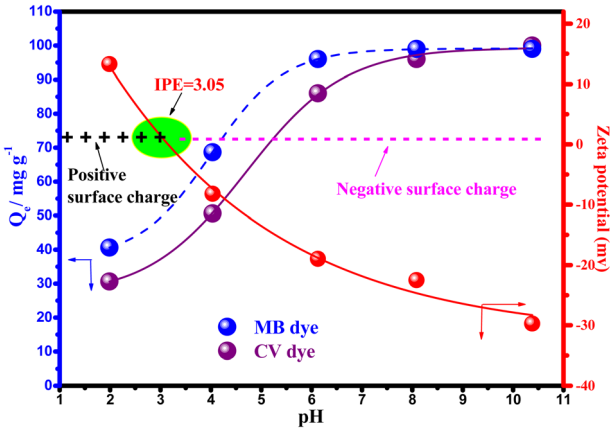

Fig. 8 Zeta potential and effect of pH on the adsorption of MB and CV dyes onto Mt@AC (Experimental conditions: C_0: 100 mg L^{-1}, Adsorbent dose = 1 g L^{-1}; contact time: 180 min; temperature = 20 °C).

From Fig. 8, it is observed that two variations are studied as a function of pH; the adsorbed quantities of MB and CV dyes and the zeta potential of Mt@AC. As clearly depicted the percentage removal of MB and CV dyes increases when the pH increases from 2 to 8. The analysis of zeta potential in Fig. 8 further shows that the surface of Mt@AC is negatively charged from pH = 3 and thus may remove the positively charged dye (MB and CV) in aqueous solution *via* electrostatic interaction. Besides, the amount of dyes adsorbed by per unit mass of Mt@AC increases with increase in pH in the range from 2.0 to 8.0 because the negative surface charge on the Mt@AC is larger at higher pH values (Fig. 8). However, at pH < 3, the sorbent surface (Mt@AC) becomes more protonated owing to more H^+ ions (zeta potential = +15.3 mV), which leads to decrease in the amount of dyes adsorbed by per unit mass of Mt@AC. This can be explained by the electrostatic repulsion between the cationic dyes (MB and CV) and the surface. More apparently, at higher pH values (8–10), the adsorption of the dyes (MB and CV) increases significantly due to the positive charges on the dyes

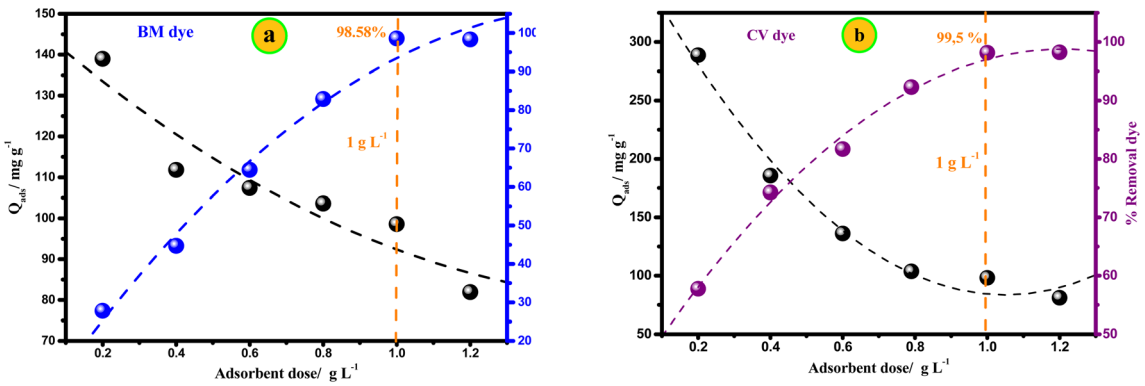

Fig. 7 Effect of adsorbent dose on adsorption of MB (a) and CV (b) dyes onto Mt@AC (experimental conditions: C_0: 100 mg L^{-1}, pH = 6.4 for MB and 6.9 for CV; contact time = 180 min; temperature = 20 °C).

ensured that they are attracted by anionic adsorbent (Mt@AC). Thus, there are strong attraction forces (electrostatic attractions) between the negative surface of the adsorbent and positive charges of dye. According to that, the mechanism of dyes adsorption onto the Mt@AC is believed to be an ion-exchange process between 3 < pH < 8 and more dominantly electrostatic attractions at higher pH values (8–10). Therefore, the optimal pH for the adsorption of the dyes (MB and CV) by adsorbent (Mt@AC) is chosen at pH 8 and used for the next investigations.

3.2.3. Effect of contact time. The contact time is an important factor in the process of dyes adsorption onto adsorbents surface. In this work, the effect of contact time at pH 8 is investigated for three concentrations 150, 250 and 400 mg L^{-1} for each dye with varied contact time (0–180 min). The obtained results are presented in Fig. 9. From this figure, it is noticed that the adsorbed quantity of each dye increases with increment in contact time until the equilibrium is obtained where the adsorption capacity remains unchangeable. Indeed, during the first minutes (for initial concentration = 250 mg L^{-1}), the adsorption capacity of CV and MB dyes increases from 198 to 233 mg g^{-1} and from 180 to 222 mg g^{-1}, respectively when the contact time increases from 5 to 15 min. This phenomenon can be explained as follows:

➢ At the first minutes of the experiment: the vacant sites on the surface of Mt@AC are in large numbers which promotes the adsorption of dyes on these sites.

➢ At the last minutes of the experiment: the vacant sites on the composite surface decrease due to their occupation by the adsorbed dye molecules, which explains the decrease in the amount of dyes adsorbed with contact time.

In addition, the remaining vacant sites on the surface of Mt@AC are difficult to be occupied due to the force of electrostatic repulsion. On the other hand, Fig. 9 shows an increase in the adsorbed quantity of dyes with the increase in the initial concentration of dyes. This phenomenon can be clarified by the increase in the possibility of collision between the dye molecules on the surface of Mt@AC composite.[7] The contact time is estimated at 30 min for the CV dye and 50 min for the MB dye.

3.2.4. Adsorption kinetics. The study of adsorption kinetics provides several keys information in order to propose the adsorption mechanism. In this work, the adsorption process of the two dyes: CV and MB, is interpreted by applying non-linear kinetic models such as: pseudo first-order and pseudo-second order[24] The non-linear forms of the equations of these models (Table 1) have been plotted and presented in Fig. 9. The choice of the best kinetic model is based on the error analysis that has been studied by the determination of the non-linear chi-square χ^2 and the Root Mean Square Error (RMSE) which are calculated respectively by eqn (7) and (9) and illustrated in Table 3. Indeed, the best model is the model with the value of R^2 is close to unity, χ^2 is close to zero and a weaker RMSE value ($R^2 \rightarrow 1$ and $\chi^2 \rightarrow 0$, RMSE lower).[43,44] The calculated kinetic parameters (K_1, K_2, $Q_{e,calc}$) obtained from the non-linear form for each model, as well as the values of the determination coefficients R^2, the values of χ^2 and RMSE are presented in Table 3. As can be seen in Table 3, the pseudo first order model is the most suitable for explaining the kinetics of adsorption of the two dyes on the surface of Mt@AC composite. Indeed, the values of the coefficients of determination R^2 are close to unity ($R^2 = 0.99$) for all the concentrations tested for the two dyes, as well as the RMSE values obtained by the pseudo first order model (0.405–6.258 for CV dye and 1.338–8.875 for MB dye) are lower than those of pseudo-second order (3.112–13.69 for CV dye and 4.983–9.848 for MB dye). Moreover, the values of chi square (χ^2) which translates the difference between the data obtained experimentally and theoretically for each model shows that the pseudo first order model has a margin of error close to zero (0.001–0.106 for CV and 0.031–0.097 for MB) than the second order model (0.066–0.508 for CV and 0.167–0.233 for MB). Another important thing which proves that the first order model described well the kinetics of adsorption of CV and MB dyes on the Mt@AC composite is the adsorbed quantities that calculated by this model are very close to that obtained experimentally (Table 3).

3.2.5. Adsorption isotherm. In this section of the adsorption isotherm, the unit of the adsorbed quantities of each dye is expressed in mmol g^{-1} so that the most adsorbed dye can be known. The adsorption isotherm for the removal of two cationic dyes by the Mt@AC composite is essential to estimate the maximum adsorption capacity as well as to propose the

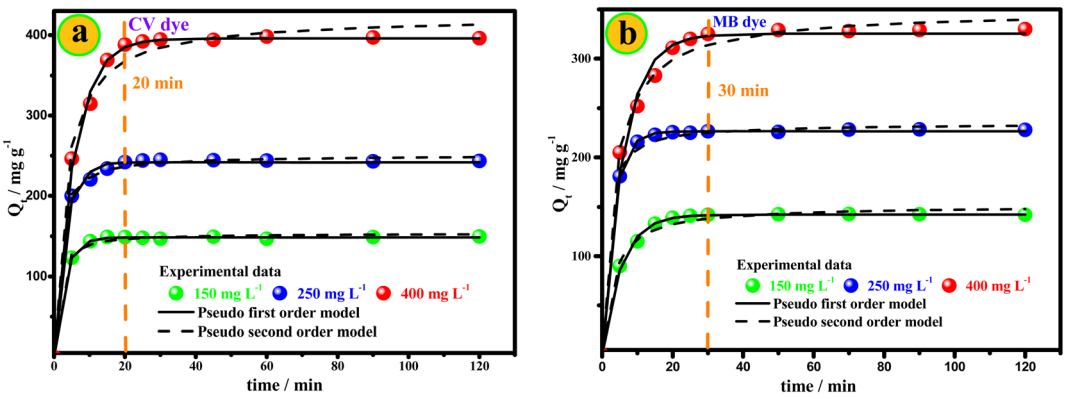

Fig. 9 Effect of contact time and kinetic modeling of the adsorption of CV (a) and MB (b) dyes onto Mt@AC (experimental conditions: $C_0 = 150$, 250 and 400 mg L^{-1}, pH = 8.0, adsorbent dose = 1 g L^{-1}; temperature = 20 °C).

Table 3 Pseudo-first-order and Pseudo-second-order model parameters for the adsorption of MB and CV onto the Mt@AC composite

Dye		CV			MB		
Initial concentration	**mg L^{-1}**	**150**	**250**	**400**	**150**	**250**	**400**
$Q_{e,exp}$	(mg g^{-1})	149.64	243.5	396.5	142.2	228.5	330.8
Pseudo-first-order							
$Q_{e,cal}$	(mg g^{-1})	149.35	241.80	395.79	142.18	226.50	325.37
k_1	(min^{-1})	0.346	0.3266	0.1796	0.1850	0.3165	0.1673
R^2	—	0.99	0.99	0.99	0.99	0.99	0.99
χ^2	—	0.0011	0.0039	0.1062	0.0316	0.0073	0.0978
RMSE	—	0.405	4.951	6.258	1.338	2.163	8.875
Pseudo-second order							
$Q_{e,cal}$	(mg g^{-1})	153.71	250.68	423.36	151.40	234.44	348.96
k_2	(g mg^{-1} min^{-1})	0.0065	0.0033	0.0007	0.0023	0.0035	0.0008
R^2	—	0.97	0.97	0.96	0.96	0.97	0.98
χ^2	—	0.0662	0.056	0.5083	0.1679	0.0940	0.2334
RMSE	—	3.112	3.635	13.698	4.983	4.802	9.848

adsorption mechanism.[14,43] The adsorption isotherm experiments are carried out at constant temperature 20 °C with adsorbent dose 1.0 g L^{-1} of Mt@AC and at optimal pH 8. The initial concentrations used for each dye is in the range of 200 to 1250 mg L^{-1} for the MB dye and 500 to 1500 mg L^{-1} for the CV dye. The experimental results obtained (Fig. 10) are fitted to the two most used models, the Freundlich (eqn 5) and the Langmuir (eqn 6) models.[26] The parameters of each model are calculated using the non-linear optimization technique to minimize the modeling error.[45] The interpretation of the obtained values in Table 4 suggests that the Langmuir model is the best model that describes the adsorption of CV and MB dyes on Mt@AC. This interpretation is based on the low values of chi-square χ^2 and RMSE and the higher values of the coefficient of determination R^2 for the Langmuir isotherm than the Freundlich model.

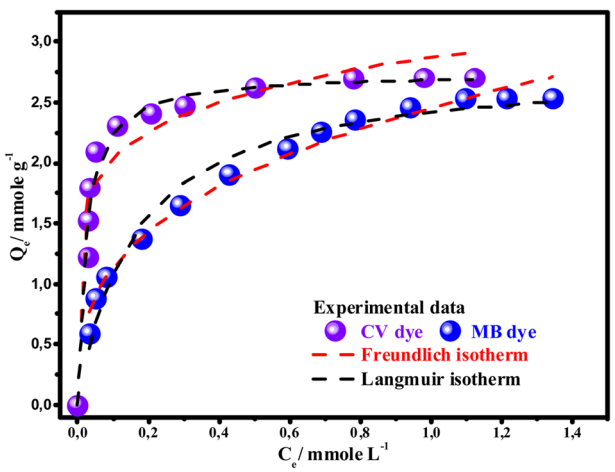

Fig. 10 Adsorption isotherm of MB and CV dyes onto Mt@AC (experimental conditions: C_0 = 200–1250 mg L^{-1} for MB dye and C_0 = 500–1500 mg L^{-1} for CV dye; pH = 8; contact time = 180 min; adsorbent dose = 1 g L^{-1}; temperature = 20 °C).

In addition, the maximum adsorption capacities obtained experimentally for the CV and MB dyes are respectively 2.7085 mmol g^{-1} (1105.6 mg g^{-1}) and 2.521 mmol g^{-1} (806.4 mg g^{-1}). These values are close to the quantities calculated using the Langmuir model 2.745 mmol g^{-1} (1110.8 mg g^{-1}) for the CV dye and 2.507 mmol g^{-1} (801.7 mg g^{-1}) for MB dye, which confirms that Langmuir isotherm is the best model explains the adsorption behavior of the two dyes on the Mt@AC composite. The confirmation that the adsorption of the two dyes is well adjusted by the Langmuir model is supported by the separation

Table 4 Isotherms parameters of the adsorption of MB and CV dyes onto the Mt@AC composite

Adsorption models	Isotherm constants CV dye	CV dye	MB dye
Langmuir	Q_m (mg g^{-1})	1110.8	801.7
	Q_m (mmol g^{-1})	2.745	2.507
	K_L(L $mmol^{-1}$)	4.40	6.400
	R_L	0.058–0.153	0.038–0.199
	χ^2	0.0077	0.0069
	RMSE	0.0562	0.0119
	R^2	0.999	0.990
Freundlich	n_F	6.70	2.99
	K_F (mmol g^{-1}) (mmol L^{-1})^n	2.876	2.458
	χ^2	0.0193	0.0140
	RMSE	0.216	0.1903
	R^2	0.93	0.96

Table 5 Adsorption capacities of MB and CV dyes on various adsorbents

Dye	Adsorbent	T (°C) pH	Q_m (mg g^{-1})	References
MB dye	Montmorillonite	20 °C pH = 7.9	327	47
	Activated carbon	25 °C pH = 7.5	324.7	48
	Natural clay mineral	20 °C pH = 7.5	100	49
	Mesoporous-activated carbon	30 °C pH = 11	143.53	44
	MMT@C nanocomposites	25 °C pH = 10	194.2	50
	Mt@AC	20 °C pH = 8	801.7	This study
CV dye	Natural clay mineral	20 °C pH = 7.5	330	49
	Zeolite-montmorillonite	25 °C pH = 9	150.516	51
	Montmorillonite	20 °C pH = 7.9	640.15	47
	Activated carbon	25 °C pH = 9	84.11	51
	Waste apricot (activated carbon)	30 °C natural pH	52.86	52
	Mt@AC	20 °C pH = 8	1110.8	This study

factor calculation R_L.[46] Indeed the value of R_L ($R_L = \frac{1}{1 + K_L C_0}$; K_L is the Langmuir constant; C_0 is initial concentration of dye) indicates whether the adsorption reaction is unfavorable ($R_L > 1$), linear ($R_L = 1$), favorable ($0 < R_L < 1$), or irreversible ($R_L = 0$). The R_L values for the CV and MB dyes presented in Table 4 show that R_L is between 0 and 1, which indicates that the adsorption of CV and MB dyes onto Mt@AC surface is a favorable process.

According to these isotherms results and the Langmuir model hypotheses cited in the literature,[5] it can be assumed that: (i) the active sites of surface adoption of the Mt@AC composite are energetically homogeneous, (ii) the adsorbed molecules form a monolayer on the composite surface (iii) no interaction exists between the adsorbed dye molecules.

On the other hand, from the values in the Table 4, it is noted that the CV dye is more adsorbed than the MB dye onto the composite surface; this behavior will be discussed in the theoretical section of this paper.

The maximum adsorption capacity of the two MB and CV dyes by Mt@AC composite was compared with that of other adsorbents reported in the literature as shown in Table 5. The adsorbent Mt@AC prepared in this work exhibits a higher adsorption capacity of the two dyes (801.7 mg g^{-1} for MB and 1110.8 mg g^{-1} for CV) compared to the other materials studied, and it can be considered a promising alternative adsorbent for the elimination of cationic dyes.

3.3. Molecular dynamics study

3.3.1. Methodology. To derive insights on the interaction mechanisms and molecular arrangements of CV and MB molecules onto the Mt@AC composite, two separate sets of molecular dynamics simulations are performed. The adsorption process of CV and MB molecules is modeled on activated carbon (AC) and Mt clay mineral respectively by constructing adequate models taking into consideration the structural texture and chemical properties from experimental results (FTIR, XRD, SEM). Based on the most energetic stable configuration of each adsorbate–adsorbent complex obtained from dynamics simulations, the interaction configurations (arrangements and interactions) are discussed and the relative affinity between adsorbent and adsorbate (*i.e.*, stability of each complex) is computed by the estimation of the interaction energy.

3.3.2. Model building and simulation details. The main groups identified on the AC surfaces are: OH and COOH which are typical of activated carbons.[16] Moreover, relying on the type of the precursor and the process of activation during the experimental production of ACs, defects can be depicted such as rings of five or seven carbon atoms and vacancies (missing sites).[53] The Scanning Electron Microscopy (SEM) image (Fig. 5) exposes an irregular surface characterized by the existence of some cavities. Thus, to simulate the AC structure, a simple porous carbon sheet is built using the results obtained from above observations. The sheet model contains 86 carbon atoms and 14 oxygen atoms. Various defective sites distributed randomly as well as hydroxyl –OH and carboxyl –COOH functional groups are incorporated in this structure. Hydroxyl groups are attached to the sheet surface and edges whereas carboxyl groups are attached to the sheet edges only. The CV, MB and AC surfaces are structured and optimized using forcite engine applied in Materials Studio (MS) 6.0 modeling package with universal force field (UFF)[54] (Fig. 11). The charges on the AC sheet are assigned through the Q_{eq} charge equilibration method and the charge distribution on the dyes molecules is obtained by the Mulliken charge analysis. The interactions between the dyes molecules and AC sheet are examined from the NVT MD simulations denoted as AC/CV and AC/MB adsorbate–adsorbent.

On the other hand, from the X-ray diffraction (XRD) patterns of the Mt@AC/CV and Mt@AC/MB powders displayed in Fig. 2, the observed decrease in the 2θ values of the first diffraction peak when compared with Mt@AC (d_{001} reflection at 7.303° 2θ) indicates that both CV and MB are integrated in the interlayer region of the Mt. The basal spacing increases during the adsorption process and reaches the values of 1.404 nm and 1.366 nm for CV and MB, respectively. Based on the results obtained from the X-ray diffraction (XRD) patterns, the intercalation of CV and MB dyes molecules within the interlayer space of the Mt lattice is modeled as following; a Mt model consists of two layers is built starting from relevant crystallographic coordinates published by Tsipursky and Drits.[55] The built pyrophyllite crystal unit cell is recreated three times in the

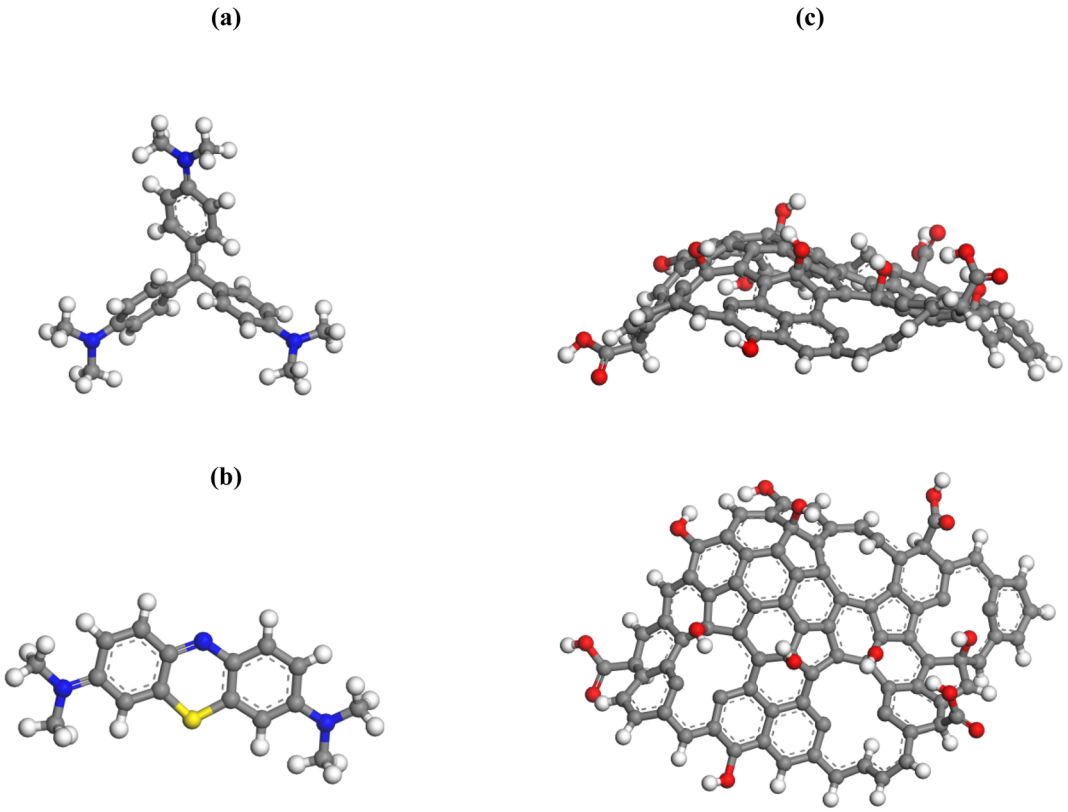

Fig. 11 Ball and stick representation of the optimized (a) CV molecule, (b) MB molecule and (c) AC surface (side and top views, respectively). Carbon, nitrogen, hydrogen, sulfur and oxygen are displayed in gray, blue, white, yellow and red, respectively.

a direction and two times in the b direction through the conditions of periodic boundary and then having a $3a \times 2b \times 1c$ super cell with the following dimensions 15.6 Å × 18.4 Å × 10.13 Å (unit cell dimensions were $a = 5.20$ Å, $b = 9.20$ Å, $c = 10.13$ Å). Thereafter, 4 Al atoms are substituted randomly by an equivalent number of Mg atoms in the octahedral sheets. The charge defect caused by the mentioned isomorphic substitutions (the charge on these sites is decreased from +3e to +2e and thus the total net charge in the Mt framework lattice has a value of −4e) is recompensed by the inclusion of $4Na^+$ counter-ion placed arbitrarily in the interlayer region (Fig. 12). Thus, the chemical unit cell composition of Mt lattice is $Na_{0.75}Si_8(Al_{3.25}Mg_{0.75})O_{20}(OH)_4$.

Next, one CV or MB molecule in their cationic forms are manually incorporated in the interlayer space by removing one Na^+ ion and thus obtaining the Mt/CV and Mt MB^{-1} adsorbate–adsorbent complexes. Each of the prepared AC/CV, AC/MB, Mt/CV and Mt MB^{-1} complexes are first annealed using "anneal" task within Forcite module. This process is consisted by heating of the system from 300 K to 500 K with temperature increments of 10 K, and then cooling to 300 K again in the same way for 20 annealing cycles. 250 MD steps of 1.0 fs are run in every heating/cooling step. At the end of each cycle the system is geometry optimized. Subsequently, MD simulations in canonical ensemble NVT (constant number of particles, volume and temperature) are run at room temperature (298 K) using COMPASS (see ESI S2†) force field to obtain the most stable configuration. During the simulations, the SMART geometry optimization algorithm is used with convergence thresholds set to 1×10^{-5} kcal mol^{-1} for convergence tolerance and 5×10^{-3} (kcal mol^{-1})/Å for maximum force. Temperature control is made by Nosé thermostat and the length of the simulations is attuned to make certain equilibration and relevant sampling. In the current study, a time step of 1 fs is used for 500 ps of molecular dynamics, during which the positions of the Na^+, Mt and AC atoms are fixed but the CV and MB are allowed to move

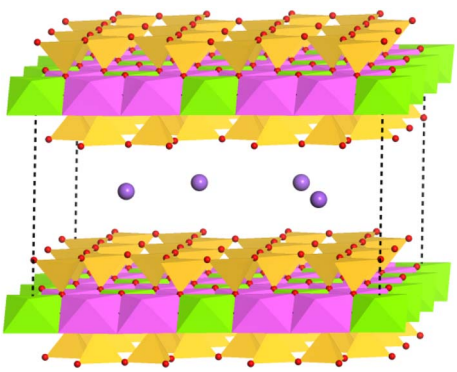

Fig. 12 Polyhedron representation of the Mt super cell lattice used in the simulations. red, pink, light green, golden and violet represent oxygen, aluminum, magnesium, silicon and sodium atoms, respectively.

consequently. The summation of Ewald method is used to treat van der Waals and the electrostatic interactions with a cutoff distance of 12 Å and accuracy of 1×10^{-5} kcal mol^{-1}, respectively.

The relative affinity between molecules in each equilibrated model gained from the conducted simulations is computed by calculation of the interaction energy (E_{int}) using the following equation:

$$E_{int} = E_{dye/surface} - E_{surface} - E_{dye} \quad (10)$$

where $E_{dye/surface}$ is the total energy of CV or MB adsorbed over the AC or Mt, $E_{surface}$ is the total energy of relaxed surface (AC or Mt) and E_{dye} is the total energy of the dye molecule (either CV or MB).

3.3.3. Adsorption process from MD simulations

3.3.3.1 Behavior of CV and MB dyes towards AC. From the conducted simulations, the most energetic stable AC/CV and AC/MB configuration snapshots (Fig. 13) show a perpendicular positioning of CV over AC surface, whereas MB molecule lies parallel on this surface.

Radial distribution function (RDF) analysis of MD simulations reveals that the hydrophobic H-bonded-to-C atoms of CV dye molecule are located at short distances from O atoms of AC (2.87 Å) (red line in Fig. 14). Whereas, in the case of MB molecule, the H(C) atoms are located at larger distances (3.35 Å) from the framework of O atoms (blue line in Fig. 14). In fact, MB molecule adsorbs on the AC surface following a parallel mode. Therefore, due to the curved form of the AC surface and the rigid structure of the MB, the interatomic distances between the surface and the MB can be varied considerably. While the perpendicular adsorption mode and the flexibility of CV molecule allows a good adaptation over the curved AC surface and thus leading to more beneficial contact. When realistic configurations are considered (more than one CV molecule has been absorbed), the adsorption process is predicted to be efficient and easier. This prediction is corresponded to the adsorbed molecules that occupy a lower space on the available surface when compared with MB molecules, which bind horizontally and therefore make the adsorption process less efficient and more difficult.

The interaction energy between the adsorbent and adsorbate, bonded (intramolecular) and non-bonded

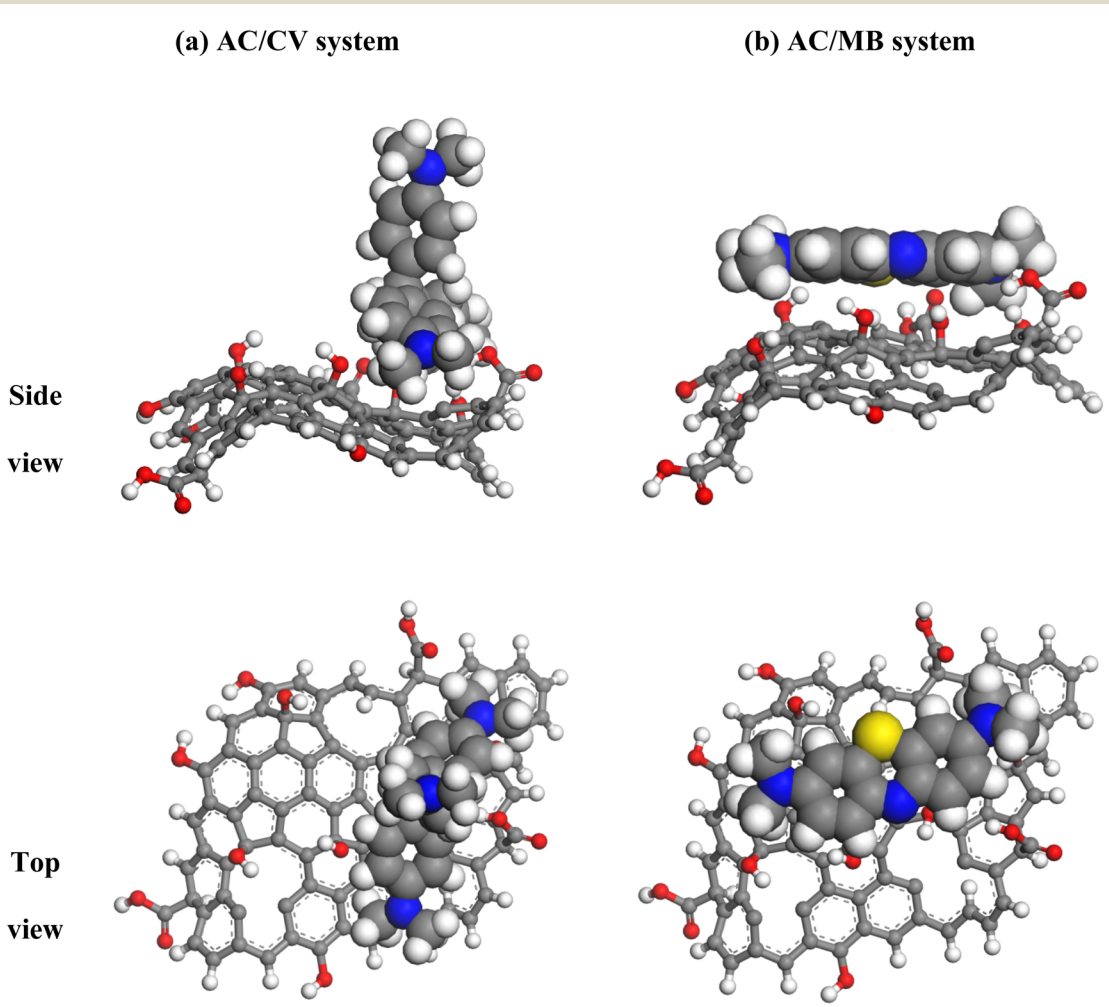

Fig. 13 Top and side views of the most energetic stable configurations of (a) CV and (b) MB (CPK model) over the AC surface (ball and stick model) from the NVT MD simulations.

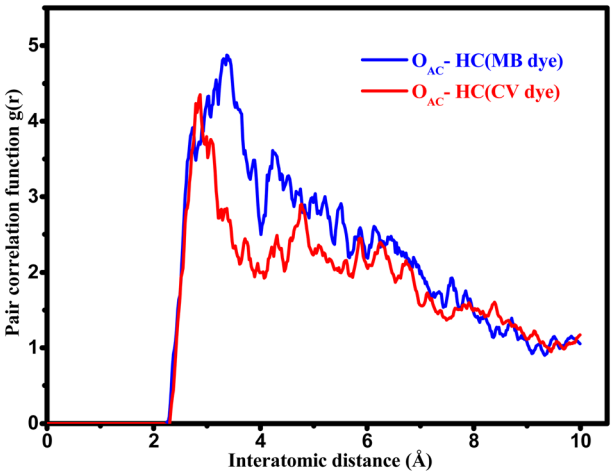

Fig. 14 Comparison of RDFs between O_{AC} (oxygen atoms on AC surface) and the different H atoms of the CV (red line) and MB (blue line) molecules.

(intermolecular) energy contributions to the total energy for each molecular configuration (*i.e.*, most stable structure from MD calculations) are summarized in Table 6.

As displayed in Table 6, the obtained E_{int} values indicate stronger interaction between CV and AC (−69.5 kcal mol^{-1}) than that between MB and AC surface (−42.7 kcal mol^{-1}), which suggests a high binding affinity of CV dye with the AC as compared with MB. In addition, the conducted calculations reveal that the intramolecular forces are mainly contributed in the total energy for both AC/CV and AC/MB complexes. For the intermolecular contribution, positive values of van der Waals forces indicate their repulsive character. Meanwhile, electrostatic interactions are found to be attractive (negative values). Therefore, electrostatic interactions are highly suggested between the AC surface which is negatively charged (owing to the existence of polar oxygen-containing functional groups) at the pH of the solution (pH = 8) and the positively charged dye molecules. On the other hand, the excessively close location of the CV molecule from the surface of AC, as revealed by the RDF analysis as well as to its highest flexibility, allows these molecules to be easily adsorbed on AC due to π–π interactions between the aromatic rings of CV molecule and AC, which leads to further stabilization of the resulting AC/CV complex. For MB molecule, the π–π interactions are highly suggested due to the large aromatic backbone of MB molecule.[56,57] However, the curved form of the AC surface and the rigid structure of the MB molecule can prevent the close contact with this surface and consequently, such interactions are expected to be weaker as compared with the case of CV. Hence, it is concluded that CV molecules are more favorable to be adsorbed onto the AC with respect to MB.

3.3.3.2 Behavior of CV and MB dyes towards montmorillonite. The COMPASS force-field[58] is used to model the molecular structure and the interaction energies of CV and MB within the interlayer space of the Mt lattice. The relative stability of the CV and MB molecules within the interlayer space of the Mt framework as a function of the interlayer distance is shown in Fig. 15. As can be seen, a significant raise of the stability (decrease of the relative energy) with increasing interlayer space up to a distance from which a continuous decrease of stability (increase of the relative energy) is observed. The results obtained from the COMPASS force-field for the most stable interlayer distances (being 13.5 Å for CV and 13.00 Å for MB) show a very good agreement with the experimentally observed interlayer distances which have values of 14.04 Å for CV and 13.66 Å for MB. Even though the used models in the simulation process do not take into account the water molecules within the interlayer space. These findings demonstrate that the

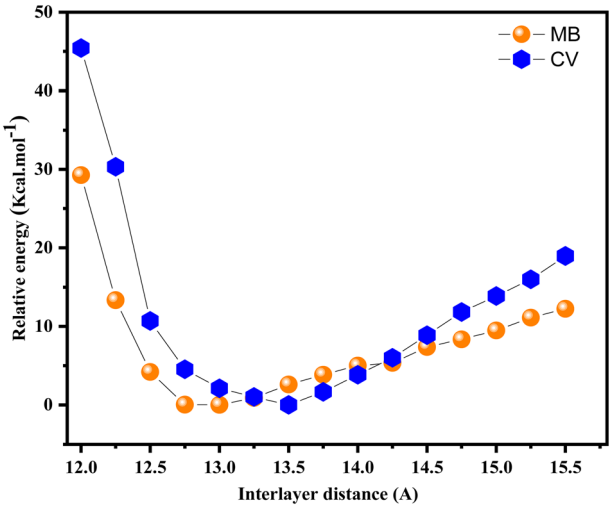

Fig. 15 Relative energy (in kcal mol^{-1}) of one CV and one MB molecule, loaded within the interlayer space of the Mt lattice as a function of the interlayer distance obtained using UFF (blue) and COMPASS (red) force-fields.

Table 6 Calculated interaction energy E_{int}, bonded and non-bonded energy contributions in most the stable adsorbate/adsorbent configurations from MD simulations

Most stable adsorbate/adsorbent configuration	E_{int} (kcal mol^{-1})	Bonded energy (kcal mol^{-1})	Non bonded energy (kcal mol^{-1})	
			van der Waals	Electrostatic
AC/CV	−69.476	75.497	27.813	−38.949
AC/MB	−42.743	24.71	6.479	−5.710
Mt/CV	−135.740	−11.425	−11.402	−72.139
Mt/MB	−57.987	14.206	−29.057	−0.718

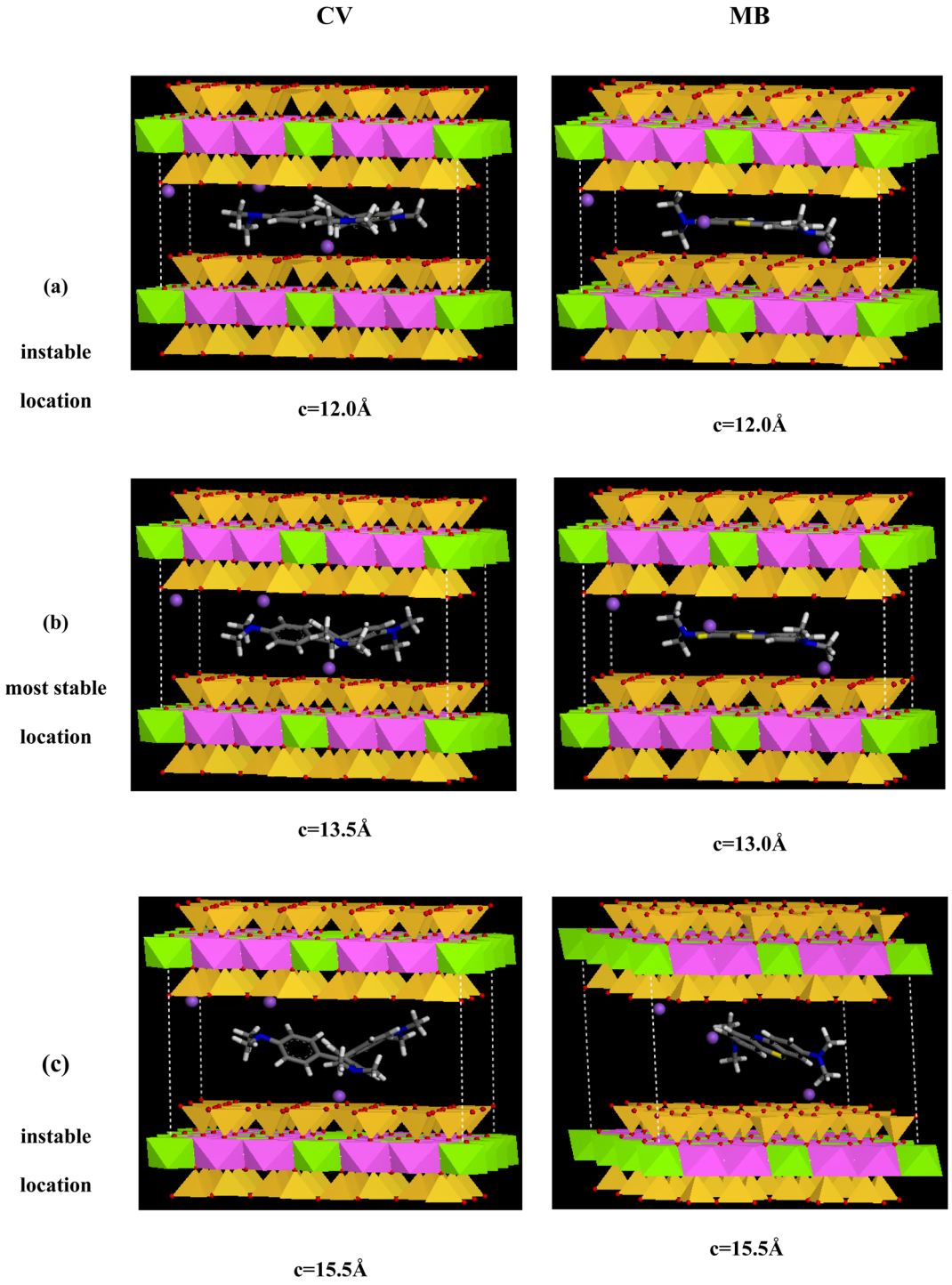

Fig. 16 Lowest energy configurations (as obtained with the COMPASS potential) of CV and MB within Mt interlayer space from the NVT MD as a function of the interlayer space: the unstable original Mt lattice with $c = 12.0$ Å (a), the most stable case with $c = 13.5$ Å and $c = 13.0$ Å for CV and MB respectively (b) and the unstable Mt lattice with large interlayer distance of 15.5 Å (c).

computational models and the setting parameters are adequate to properly simulate the swelling of montmorillonite during the inclusion of the dyes molecules.

As observed in Fig. 15, an increase of the interlayer space leads to cumulative stabilization of the Mt/CV and Mt MB^{-1} complexes, since a progressive larger space is available to accommodate the guest CV and MB cations. When the CV and MB cations are loaded in the original montmorillonite framework (of the Mt@AC composite) with initial "*c*" parameter of 12.0 Å (see Fig. 16a), RDF curve depicted in Fig. 17a reveals too short distances between oxygen atoms of the siloxane interlayer surfaces (O_{Mt}) and the different H(C) atoms of both CV (2.41 Å)

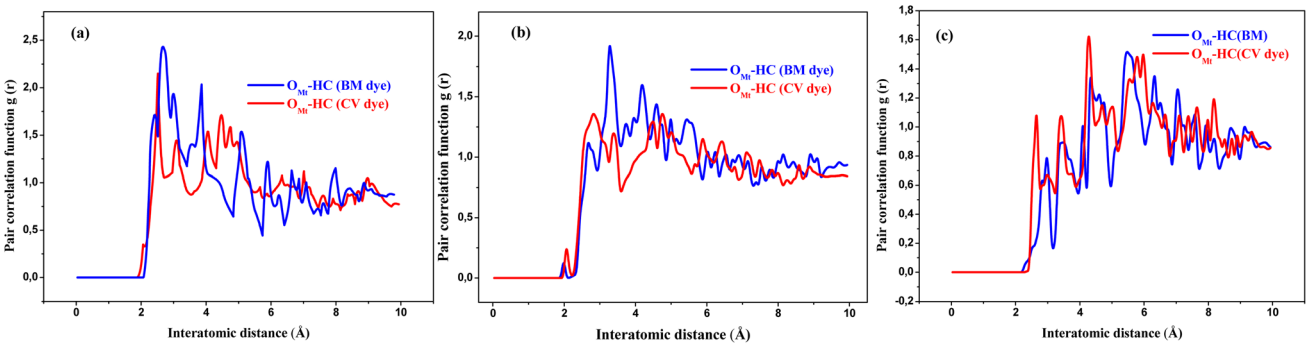

Fig. 17 Comparison of RDFs between O_{Mt} (O atoms in the interlayer space) and the different H atoms of the CV (red line) and MB (blue line) molecules docked within the Mt lattice with $c = 12.0$ Å (a), $c = 13.5$ Å and $c = 13.0$ Å for CV and MB respectively (b) and $c = 15.5$ Å (c).

and MB (2.48 Å) molecules. This causes a significant steric repulsions and thus less stable structures.

The most stable configurations of the Mt/CV and Mt/MB complexes, as calculated by the COMPASS force field, are obtained when CV and MB cations are loaded in the Mt lattice with c values of 13.50 Å and 13.0 Å, respectively (Fig. 16b). In this case, the distances between O–Mt atoms and the H atoms are relatively large (2.81 Å and 3.26 Å for CV and MB respectively as displayed in Fig. 17b). The interlayer space in the Mt lattice seems to be large enough to accommodate the dyes molecules and consequently prevents steric repulsions. The interaction energy E_{int} values shown in Table 6 indicate stronger interaction of CV with both layers of the Mt lattice (-135.7 kcal mol^{-1}) than that for MB with these layers (-57.9 kcal mol^{-1}). Moreover, van der Waals and electrostatic forces are found to be attractive (have negative values) for the both systems, which indicates high stability of the resulting complexes. However, a decrease in the stability of the Mt/CV and Mt/MB complexes is observed again when the interlayer space is further increased (Fig. 15). RDF results displayed in Fig. 17c which are obtained from analysis of Mt lattice with large interlayer space ($c = 15.5$ Å as an example) show that H(C) atoms are too far to interact with the O_{Mt} atoms (4.23 Å and 4.31 Å for CV and MB, respectively). In this case, the interlayer distance is too large to allow strong interactions, which results in a lower stability of the obtained complexes (Fig. 16c).

4. Conclusion

In this paper, an eco-friendly nanocomposite Mt@AC is synthesized and characterized utilizing the Moroccan natural montmorillonite clay and wheat straw. The nanocomposite is used as potential adsorbent to remove two cationic dyes; methylene blue and crystal violet from aqueous solutions. The removal of the two dyes by adsorption on Mt@AC composite increases with pH and contact time which needs around 30 min for MB dye and 20 min for CV dye to reach equilibrium. The equilibrium adsorption isotherm results correlate well with the Langmuir isotherm model with a maximum adsorption capacity of 801.7 mg g^{-1} for the MB and 1110.8 mg g^{-1} for the CV at pH 8. The kinetic data is well fitted with pseudo-first order kinetic model for the two dyes with coefficient of determination R^2 close to unity, non-linear chi-square χ^2 close to zero and lower Root Mean Square Error RMSE. The intermolecular interaction energy E_{int} calculations and RDF analysis retrieved from the MD simulations demonstrate a stronger interaction of the CV molecule with both AC sheet and Mt framework as compared with MB. The simulation results are consistent with the experimental outcome, which proves the accuracy and feasibility of the simulation calculation.

Conflicts of interest

There are no conflicts to declare.

Acknowledgements

We would like to thank Dr Samira Dalbouha from the Faculty of Science Ait Melloul Ibn Zohr University-Morocco for their help and support in the revision phase of this work.

References

1 R. Haounati, H. Ouachtak, R. El Haouti, S. Akhouairi, F. Largo, F. Akbal, A. Benlhachemi, A. Jada and A. A. Addi, Elaboration and properties of a new SDS/CTAB@Montmorillonite organoclay composite as a superb adsorbent for the removal of malachite green from aqueous solutions, *Sep. Purif. Technol.*, 2021, **255**, 117335, DOI: 10.1016/j.seppur.2020.117335.

2 M. R. Bilad, Membrane bioreactor for domestic wastewater treatment: principles, challenges and future research directions, *Indones. J. Sci. Technol.*, 2017, **2**, 97, DOI: 10.17509/ijost.v2i1.5993.

3 M. Anbia, N. Mohammadi and K. Mohammadi, Fast and efficient mesoporous adsorbents for the separation of toxic compounds from aqueous media, *J. Hazard. Mater.*, 2010, **176**, 965–972, DOI: 10.1016/j.jhazmat.2009.11.135.

4 F. Alakhras, E. Alhajri, R. Haounati, H. Ouachtak, A. A. Addi and T. A. Saleh, A comparative study of photocatalytic degradation of Rhodamine B using natural-based zeolite

composites, *Surf. Interfaces*, 2020, **20**, 100611, DOI: 10.1016/j.surfin.2020.100611.

5 S. Akhouairi, H. Ouachtak, A. A. Addi, A. Jada and J. Douch, Natural Sawdust as Adsorbent for the Eriochrome Black T Dye Removal from Aqueous Solution, Water, Air, *Water, Air, Soil Pollut.*, 2019, **230**, 181, DOI: 10.1007/s11270-019-4234-6.

6 H. Ouachtak, S. Akhouairi, R. Haounati, A. A. Addi, A. Jada, M. L. Taha and J. Douch, 3,4-Dihydroxybenzoic acid removal from water by goethite modified natural sand column fixed-bed: experimental study and mathematical modeling, *Desalin. Water Treat.*, 2020, **194**, 439–449, DOI: 10.5004/dwt.2020.25562.

7 R. El Haouti, H. Ouachtak, A. El Guerdaoui, A. Amedlous, E. Amaterz, R. Haounati, A. A. Addi, F. Akbal, N. El Alem and M. L. Taha, Cationic dyes adsorption by Na-Montmorillonite Nano Clay: Experimental study combined with a theoretical investigation using DFT-based descriptors and molecular dynamics simulations, *J. Mol. Liq.*, 2019, **290**, 111139, DOI: 10.1016/j.molliq.2019.111139.

8 F. Alakhras, H. Ouachtak, E. Alhajri, R. Rehman, G. Al-Mazaideh, I. Anastopoulos and E. C. Lima, Adsorptive Removal of Cationic Rhodamine B Dye from Aqueous Solutions Using Chitosan-Derived Schiff Base, *Sep. Sci. Technol.*, 2022, **57**, 542–554, DOI: 10.1080/01496395.2021.1931326.

9 D. Shen, J. Fan, W. Zhou, B. Gao, Q. Yue and Q. Kang, Adsorption kinetics and isotherm of anionic dyes onto organo-bentonite from single and multisolute systems, *J. Hazard. Mater.*, 2009, **172**, 99–107, DOI: 10.1016/j.jhazmat.2009.06.139.

10 R. Haounati, A. El Guerdaoui, H. Ouachtak, R. El Haouti, A. Bouddouch, N. Hafid, B. Bakiz, D. M. F. Santos, M. Labd Taha, A. Jada and A. Ait Addi, Design of direct Z-scheme superb magnetic nanocomposite photocatalyst Fe_3O_4/Ag_3PO_4@Sep for hazardous dye degradation, *Sep. Purif. Technol.*, 2021, **277**, 119399, DOI: 10.1016/j.seppur.2021.119399.

11 C. V. Reddy, R. Koutavarapu, K. R. Reddy, N. P. Shetti, T. M. Aminabhavi and J. Shim, Z-scheme binary 1D ZnWO4 nanorods decorated 2D $NiFe_2O_4$ nanoplates as photocatalysts for high efficiency photocatalytic degradation of toxic organic pollutants from wastewater, *J. Environ. Manage.*, 2020, **268**, 110677, DOI: 10.1016/j.jenvman.2020.110677.

12 F. Largo, R. Haounati, S. Akhouairi, H. Ouachtak, R. El Haouti, A. El Guerdaoui, N. Hafid, D. M. F. Santos, F. Akbal, A. Kuleyin, A. Jada and A. A. Addi, Adsorptive removal of both cationic and anionic dyes by using sepiolite clay mineral as adsorbent: Experimental and molecular dynamic simulation studies, *J. Mol. Liq.*, 2020, **318**, 114247, DOI: 10.1016/j.molliq.2020.114247.

13 R. Haounati, F. Alakhras, H. Ouachtak, T. A. Saleh, G. Al-Mazaideh, E. Alhajri, A. Jada, N. Hafid and A. A. Addi, Synthesized of Zeolite@Ag_2O Nanocomposite as Superb Stability Photocatalysis Toward Hazardous Rhodamine B Dye from Water, *Arabian J. Sci. Eng.*, 2023, **48**, 169–179, DOI: 10.1007/s13369-022-06899-y.

14 H. Ouachtak, R. El Haouti, A. El Guerdaoui, R. Haounati, E. Amaterz, A. A. Addi, F. Akbal and M. L. Taha, Experimental and molecular dynamics simulation study on the adsorption of Rhodamine B dye on magnetic montmorillonite composite γ-Fe_2O_3@Mt, *J. Mol. Liq.*, 2020, **309**, 113142, DOI: 10.1016/j.molliq.2020.113142.

15 R. Ait Akbour, H. Ouachtak, A. Jada, S. Akhouairi, A. Ait Addi, J. Douch and M. Hamdani, Humic acid covered alumina as adsorbent for the removal of organic dye from coloured effluents, *Desalin. Water Treat.*, 2018, **112**, 207–217, DOI: 10.5004/dwt.2018.22006.

16 S.-A. Sajjadi, A. Meknati, E. C. Lima, G. L. Dotto, D. I. Mendoza-Castillo, I. Anastopoulos, F. Alakhras, E. I. Unuabonah, P. Singh and A. Hosseini-Bandegharaei, A novel route for preparation of chemically activated carbon from pistachio wood for highly efficient Pb(II) sorption, *J. Environ. Manage.*, 2019, **236**, 34–44, DOI: 10.1016/j.jenvman.2019.01.087.

17 R. A. Raso, M. Zeltner and W. J. Stark, Indoor Air Purification Using Activated Carbon Adsorbers: Regeneration Using Catalytic Combustion of Intermediately Stored VOC, *Ind. Eng. Chem. Res.*, 2014, **53**, 19304–19312, DOI: 10.1021/ie503851q.

18 R. I. Kosheleva, A. C. Mitropoulos and G. Z. Kyzas, Synthesis of activated carbon from food waste, *Environ. Chem. Lett.*, 2019, **17**, 429–438, DOI: 10.1007/s10311-018-0817-5.

19 Y. Ma, Comparison of Activated Carbons Prepared from Wheat Straw via $ZnCl_2$ and KOH Activation, *Waste Biomass Valorization*, 2017, **8**, 549–559, DOI: 10.1007/s12649-016-9640-z.

20 Y.-P. Huang, C.-H. Hou, H.-C. Hsi and J.-W. Wu, Optimization of highly microporous activated carbon preparation from Moso bamboo using central composite design approach, *J. Taiwan Inst. Chem. Eng.*, 2015, **50**, 266–275, DOI: 10.1016/j.jtice.2014.12.019.

21 P. Nowicki, J. Kazmierczak and R. Pietrzak, Comparison of physicochemical and sorption properties of activated carbons prepared by physical and chemical activation of cherry stones, *Powder Technol.*, 2015, **269**, 312–319, DOI: 10.1016/j.powtec.2014.09.023.

22 R. Zhu, Q. Chen, Q. Zhou, Y. Xi, J. Zhu and H. He, Adsorbents based on montmorillonite for contaminant removal from water: A review, *Appl. Clay Sci.*, 2016, **123**, 239–258, DOI: 10.1016/j.clay.2015.12.024.

23 E. D. Revellame, D. L. Fortela, W. Sharp, R. Hernandez and M. E. Zappi, Adsorption kinetic modeling using pseudo-first order and pseudo-second order rate laws: A review, *Clean. Eng.Technol.*, 2020, **1**, 100032, DOI: 10.1016/j.clet.2020.100032.

24 G. Blanchard, M. Maunaye and G. Martin, Removal of heavy metals from waters by means of natural zeolites, *Water Res.*, 1984, **18**, 1501–1507, DOI: 10.1016/0043-1354(84)90124-6.

25 C. Sheindorf, M. Rebhun and M. Sheintuch, A Freundlich-type multicomponent isotherm, *J. Colloid Interface Sci.*, 1981, **79**, 136–142, DOI: 10.1016/0021-9797(81)90056-4.

26 I. Langmuir, The constitution and fundamental properties of solids and liquids. part i. solids, *J. Am. Chem. Soc.*, 1916, **38**, 2221–2295, DOI: 10.1021/ja02268a002.

27 H. N. Tran, S.-J. You, A. Hosseini-Bandegharaei and H.-P. Chao, Mistakes and inconsistencies regarding adsorption of contaminants from aqueous solutions: A critical review, *Water Res.*, 2017, **120**, 88–116, DOI: 10.1016/j.watres.2017.04.014.

28 J. C. Ng, W. Cheung and G. McKay, Equilibrium Studies of the Sorption of Cu(II) Ions onto Chitosan, *J. Colloid Interface Sci.*, 2002, **255**, 64–74, DOI: 10.1006/jcis.2002.8664.

29 S. Parimal, M. Prasad and U. Bhaskar, Prediction of Equilibrium Sorption Isotherm: Comparison of Linear and Nonlinear Methods, *Ind. Eng. Chem. Res.*, 2010, **49**, 2882–2888, DOI: 10.1021/ie9013343.

30 K. Wang, H. Ma, S. Pu, C. Yan, M. Wang, J. Yu, X. Wang, W. Chu and A. Zinchenko, Hybrid porous magnetic bentonite-chitosan beads for selective removal of radioactive cesium in water, *J. Hazard. Mater.*, 2019, **362**, 160–169, DOI: 10.1016/j.jhazmat.2018.08.067.

31 F. Zahran, H. H. El-Maghrabi, G. Hussein and S. M. Abdelmaged, Fabrication of bentonite based nanocomposite as a novel low cost adsorbent for uranium ion removal, *Environ. Nanotechnol., Monit. Manage.*, 2019, **11**, 100205, DOI: 10.1016/j.enmm.2018.100205.

32 A. Kumar, P. Raizada, P. Singh, R. V Saini, A. K. Saini and A. Hosseini-Bandegharaei, Perspective and status of polymeric graphitic carbon nitride based Z-scheme photocatalytic systems for sustainable photocatalytic water purification, *Chem. Eng. J.*, 2020, **391**, 123496, DOI: 10.1016/j.cej.2019.123496.

33 N. Horri, E. S. Sanz-Pérez, A. Arencibia, R. Sanz, N. Frini-Srasra and E. Srasra, Amine grafting of acid-activated bentonite for carbon dioxide capture, *Appl. Clay Sci.*, 2019, **180**, 105195, DOI: 10.1016/j.clay.2019.105195.

34 S. Saja, A. Bouazizi, B. Achiou, H. Ouaddari, A. Karim, M. Ouammou, A. Aaddane, J. Bennazha and S. Alami Younssi, Fabrication of low-cost ceramic ultrafiltration membrane made from bentonite clay and its application for soluble dyes removal, *J. Eur. Ceram. Soc.*, 2020, **40**, 2453–2462, DOI: 10.1016/j.jeurceramsoc.2020.01.057.

35 A. E. Gabor, C. M. Davidescu, A. Negrea, M. Ciopec, M. Butnariu, C. Ianasi, C. Muntean and P. Negrea, Lanthanum Separation from Aqueous Solutions Using Magnesium Silicate Functionalized with Tetrabutylammonium Dihydrogen Phosphate, *J. Chem. Eng. Data*, 2016, **61**, 535–542, DOI: 10.1021/acs.jced.5b00687.

36 N. Mojoudi, N. Mirghaffari, M. Soleimani, H. Shariatmadari, C. Belver and J. Bedia, Phenol adsorption on high microporous activated carbons prepared from oily sludge: equilibrium, kinetic and thermodynamic studies, *Sci. Rep.*, 2019, **9**, 19352, DOI: 10.1038/s41598-019-55794-4.

37 J. Bedia, M. Peñas-Garzón, A. Gómez-Avilés, J. J. Rodriguez and C. Belver, Review on Activated Carbons by Chemical Activation with $FeCl_3$, *C — J. Carbon Res.*, 2020, **6**, 21, DOI: 10.3390/c6020021.

38 K. A. Cychosz and M. Thommes, Progress in the Physisorption Characterization of Nanoporous Gas Storage Materials, *Engineering*, 2018, **4**, 559–566, DOI: 10.1016/j.eng.2018.06.001.

39 H. Ouachtak, A. El Guerdaoui, R. Haounati, S. Akhouairi, R. El Haouti, N. Hafid, A. Ait Addi, B. Šljukić, D. M. F. Santos and M. L. Taha, Highly efficient and fast batch adsorption of orange G dye from polluted water using superb organo-montmorillonite: Experimental study and molecular dynamics investigation, *J. Mol. Liq.*, 2021, **335**, 116560, DOI: 10.1016/j.molliq.2021.116560.

40 E. Al Abbad and F. Alakhras, Removal of Dye Acid Red 1 from Aqueous Solutions Using Chitosan-iso-Vanillin Sorbent Material, Indones, *J. Sci. Technol.*, 2020, **5**, 352–365, DOI: 10.17509/ijost.v5i3.24986.

41 N. Thinakaran, P. Panneerselvam, P. Baskaralingam, D. Elango and S. Sivanesan, Equilibrium and kinetic studies on the removal of Acid Red 114 from aqueous solutions using activated carbons prepared from seed shells, *J. Hazard. Mater.*, 2008, **158**, 142–150, DOI: 10.1016/j.jhazmat.2008.01.043.

42 G. Crini, H. Peindy, F. Gimbert and C. Robert, Removal of C.I. Basic Green 4 (Malachite Green) from aqueous solutions by adsorption using cyclodextrin-based adsorbent: Kinetic and equilibrium studies, *Sep. Purif. Technol.*, 2007, **53**, 97–110, DOI: 10.1016/j.seppur.2006.06.018.

43 H. N. Tran, F. Tomul, N. Thi Hoang Ha, D. T. Nguyen, E. C. Lima, G. T. Le, C.-T. Chang, V. Masindi and S. H. Woo, Innovative spherical biochar for pharmaceutical removal from water: Insight into adsorption mechanism, *J. Hazard. Mater.*, 2020, **394**, 122255, DOI: 10.1016/j.jhazmat.2020.122255.

44 F. Marrakchi, M. J. Ahmed, W. A. Khanday, M. Asif and B. H. Hameed, Mesoporous-activated carbon prepared from chitosan flakes via single-step sodium hydroxide activation for the adsorption of methylene blue, *Int. J. Biol. Macromol.*, 2017, **98**, 233–239, DOI: 10.1016/j.ijbiomac.2017.01.119.

45 M. Hadi, M. R. Samarghandi and G. McKay, Equilibrium two-parameter isotherms of acid dyes sorption by activated carbons: Study of residual errors, *Chem. Eng. J.*, 2010, **160**, 408–416, DOI: 10.1016/j.cej.2010.03.016.

46 K. R. Hall, L. C. Eagleton, A. Acrivos and T. Vermeulen, Pore- and Solid-Diffusion Kinetics in Fixed-Bed Adsorption under Constant-Pattern Conditions, *Ind. Eng. Chem. Fundam.*, 1966, **5**, 212–223, DOI: 10.1021/i160018a011.

47 G. Rytwo, Enthalpies of adsorption of methylene blue and crystal violet to montmorillonite, *J. Therm. Anal. Calorim.*, 2003, **71**, 751–759, DOI: 10.1023/A:1023309806214.

48 J. Gao, Y. Qin, T. Zhou, D. Cao, P. Xu, D. Hochstetter and Y. Wang, Adsorption of methylene blue onto activated carbon produced from tea (Camellia sinensis L.) seed shells: kinetics, equilibrium, and thermodynamics studies, *J. Zhejiang Univ., Sci., B*, 2013, **14**, 650–658, DOI: 10.1631/jzus.B12a0225.

49 O. Sakin Omer, M. A. Hussein, B. H. M. Hussein and A. Mgaidi, Adsorption thermodynamics of cationic dyes (methylene blue and crystal violet) to a natural clay mineral from aqueous solution between 293.15 and 323.15 K, *Arabian J. Chem.*, 2018, **11**, 615–623, DOI: **10.1016/j.arabjc.2017.10.007**.

50 L. Ai and L. Li, Efficient removal of organic dyes from aqueous solution with ecofriendly biomass-derived carbon@montmorillonite nanocomposites by one-step hydrothermal process, *Chem. Eng. J.*, 2013, **223**, 688–695, DOI: **10.1016/j.cej.2013.03.015**.

51 M. Sarabadan, H. Bashiri and S. M. Mousavi, Adsorption of crystal violet dye by a zeolite-montmorillonite nano-adsorbent: modelling, kinetic and equilibrium studies, *Clay Miner.*, 2019, **54**, 357–368, DOI: **10.1180/clm.2019.48**.

52 Y. Önal, Kinetics of adsorption of dyes from aqueous solution using activated carbon prepared from waste apricot, *J. Hazard. Mater.*, 2006, **137**, 1719–1728, DOI: **10.1016/j.jhazmat.2006.05.036**.

53 D. Bahamon, L. Carro, S. Guri and L. F. Vega, Computational study of ibuprofen removal from water by adsorption in realistic activated carbons, *J. Colloid Interface Sci.*, 2017, **498**, 323–334, DOI: **10.1016/j.jcis.2017.03.068**.

54 A. K. Rappe, C. J. Casewit, K. S. Colwell, W. A. Goddard and W. M. Skiff, UFF, a full periodic table force field for molecular mechanics and molecular dynamics simulations, *J. Am. Chem. Soc.*, 1992, **114**, 10024–10035, DOI: **10.1021/ja00051a040**.

55 S. I. Tsipursky and V. A. Drits, The distribution of octahedral cations in the 2:1 layers of dioctahedral smectites studied by oblique-texture electron diffraction, *Clay Miner.*, 1984, **19**, 177–193, DOI: **10.1180/claymin.1984.019.2.05**.

56 A. M. M. Vargas, A. L. Cazetta, M. H. Kunita, T. L. Silva and V. C. Almeida, Adsorption of methylene blue on activated carbon produced from flamboyant pods (Delonix regia): Study of adsorption isotherms and kinetic models, *Chem. Eng. J.*, 2011, **168**, 722–730, DOI: **10.1016/j.cej.2011.01.067**.

57 C. Moreno-Castilla, Adsorption of organic molecules from aqueous solutions on carbon materials, *Carbon*, 2004, **42**, 83–94, DOI: **10.1016/j.carbon.2003.09.022**.

58 H. Sun, COMPASS: An ab Initio Force-Field Optimized for Condensed-Phase ApplicationsOverview with Details on Alkane and Benzene Compounds, *J. Phys. Chem. B*, 1998, **102**, 7338–7364, DOI: **10.1021/jp980939v**.